International Journal of Biomathematics Vol. 11, No. 3 (2018) 1850034 (23 pages) © World Scientific Publishing Company DOI: 10.1142/S1793524518500341



# A multi-scale cholera model linking between-host and within-host dynamics

Chayu Yang\*, Drew Posny<sup>†</sup>, Feng Bao\* and Jin Wang\*, ‡,§

\*Department of Mathematics

University of Tennessee at Chattanooga

Chattanooga TN 37403, USA

†NSF Center for Integrated Pest Management

North Carolina State University

Raleigh NC 27606, USA

†jin-wanq02@utc.edu

Received 9 October 2017 Accepted 6 February 2018 Published 12 March 2018

We propose a multi-scale modeling framework to investigate the transmission dynamics of cholera. At the population level, we employ a SIR model for the between-host transmission of the disease. At the individual host level, we describe the evolution of the pathogen within the human body. The between-host and within-host dynamics are connected through an environmental equation that characterizes the growth of the pathogen and its interaction with the hosts outside the human body. We put a special emphasis on the within-host dynamics by making a distinction for each individual host. We conduct both mathematical analysis and numerical simulation for our model in order to explore various scenarios associated with cholera transmission and to better understand the complex, multi-scale disease dynamics.

Keywords: Cholera; equilibrium; stability; multi-scale modeling.

Mathematics Subject Classification 2010: 92D30, 34A34

#### 1. Introduction

Cholera, an acute diarrhoeal disease caused by the bacterium *Vibrio Cholerae*, continues to plague populations in developing countries with limited access to safe water and sanitation resources, as evidenced by the on-going cholera outbreak in Yemen where more than 770,000 cases have been reported by WHO [25] as of 1 October 2017.

In order to understand the fundamental mechanisms in cholera transmission and to quantify effective prevention and intervention strategies, a large number

<sup>§</sup>Corresponding author.

of mathematical models have been published (see e.g. [3, 5, 8, 10–12, 15, 19–22, 26]). Almost all of these studies are concerned with the between-host transmission and spread at the population level, and very little effort has been devoted to the within-host dynamics of cholera, partly due to the complication of the biochemical and genetic interactions that occur within the human body. As a consequence, some important information in cholera dynamics is missing from such studies; for example, how does the virulence of the pathogens (i.e. the vibrios) change inside the human body, and how does the within-host evolution of the pathogens impact the population-level disease transmission?

In a recent study [24], the authors proposed a within-host cholera model to describe the evolution of vibrios and their interaction with the cholera-toxin phage (a virus that is important in the pathogenesis of the *Vibrio cholerae*) within the human body. The connection between the within-host dynamics and the between-host disease transmission, however, was not discussed. A multi-scale cholera model that considers the between-host and within-host interactions was proposed in [23]. In that work, the within-host dynamics take a simplistic form: a single equation characterizing the increased toxicity of the vibrios within an "average" (or, typical) infected individual. Distinctions among different human hosts were not considered. We also mention that there have been several mathematical models published for the immuno-epidemiological dynamics of other types of diseases; for example, a recent study on malaria can be found in [4].

Our present work aims to extend the work in [23], in an effort to fill the knowledge gap in linking the between-host and within-host cholera dynamics while taking into account the heterogeneity among different individual hosts. In our modeling framework, we distinguish two types of vibrios relevant to cholera infection: the environmental vibrios and the human vibrios [23, 24], based on their toxicity, or infectivity. The environmental vibrios have relatively low infectivity, whereas the human vibrios (developed within the human body) typically have an infectivity much higher (up to 700-fold) than their environmental counterparts [10, 13]. Typically, due to the contacts between the hosts and the contaminated water or food, vibrios from the environment are ingested into the human body. Through a series of biological, chemical and genetic interactions during the passage of the bacteria through the human gastrointestinal tract, the environmental vibrios are transferred to human vibrios with much higher infectivity/toxicity that could directly lead to human cholera symptoms [6, 9], among which profuse diarrhea and massive fluid loss are most common.

A challenge in the design of effective prevention and intervention strategies for cholera (perhaps also for many other infectious diseases) is the highly heterogeneous pattern in the host response, individual symptoms, and transmission of the disease. These are closely related to the distinct health conditions among different human individuals. For example, some people may not easily become infected with cholera due to the strong immune system inside their bodies or the cholera vaccines they previously receive, whereas young children, old people, and those with poor health are much more vulnerable to cholera and likely exhibit severe infections.

A comprehensive description of the within-host cholera dynamics that covers all details of the pathogen evolution and transformation inside the human body, while including the individual distinctions across a large host population, would lead to highly complicated dynamical systems that are challenging to analyze or compute. Alternatively, a popular approach in disease modeling is to utilize the agent-based modeling and simulation technique, where multiple agents reside in networks and interact with each other according to a set of heuristic rules, with an aim of creating or predicting the complex overall system behavior [2, 14]. Advantages of the agent-based modeling include high flexibility and natural incorporation of heterogeneity [16, 18]. However, the nature of the agent-based framework makes it mathematically intractable, and the only way to implement/analyze such a model is through numerical simulation. The overall computational efforts can become prohibitively expensive when the number of interacting agents is large.

In this paper, we propose a novel deterministic modeling framework to connect the between-host and within-host dynamics of cholera, while keeping the model mathematically and computationally manageable. On the population level, we utilize a Susceptible–Infected–Recovered-Bacteria (SIR-B) model to describe the disease transmission and the interaction between human hosts and environmental pathogens. On the individual host level, we treat each individual as a separate compartment represented by an equation that describes the evolution from environmental vibrios to human vibrios within the human body. Within each individual host, our modeling approach is coarse-grained as the dynamics are described by a single equation characterizing the essential pathogen development from a lower-infectious state to a hyper-infectious state. However, since each host is separately modeled, distinctions among different individuals can be naturally incorporated to reflect the heterogeneity of the within-host dynamics.

In this study, we first describe our multi-scale model, and then conduct mathematical analysis and numerical simulation. Our primary focus is the autonomous system where each parameter is fixed, which enables us to conduct a thorough mathematical analysis on the equilibria and their local and global dynamics. In the numerical part, we use the simulation results to verify the analytical predictions on the autonomous system. Then, we allow the key parameters associated with the within-host dynamics to vary with time, to emphasize the feedback mechanism that links the between-host and within-host dynamics. This scenario represents a dynamic, or "adaptive", multi-scale modeling approach for cholera. We conduct careful numerical simulation to this dynamic scenario and compare the results to those from the autonomous case. Finally, we conclude the paper with some discussion.

## 2. Model and Analysis

#### 2.1. Equations

The between-host dynamics are described by the following Susceptible–Infected–Recovered (SIR) model:

$$\frac{dS}{dt} = \mu N - \beta_H S I - \beta_L S B - \mu S,$$

$$\frac{dI}{dt} = \beta_H S I + \beta_L S B - (\gamma + \mu) I,$$

$$\frac{dR}{dt} = \gamma I - \mu R,$$
(2.1)

where B is the concentration of the bacteria  $Vibrio\ cholerae$  in the contaminated water. We assume that the natural birth and death rates for human hosts are the same and denoted by  $\mu$ . Meanwhile, we denote the human-to-human and environment-to-human transmission rates by  $\beta_H$  and  $\beta_L$ , respectively. In addition,  $\gamma$  denotes the recovery rate from the infection. The total population, N = S + I + R, remains a constant in our model and, thus, we may drop the equation for R in the analysis of the model. We further assume that N is an integer in this study.

To emphasize the distinctions among human individuals in the within-host dynamics, we formulate an equation for each individual host:

$$\frac{dZ_i}{dt} = c_i B - \xi_i Z_i, \quad i = 1, 2, \dots, N.$$
 (2.2)

Here  $Z_i$  represents the concentration of human vibrios within the body of the *i*th individual,  $i=1,2,\ldots,N$ . The environmental vibrios that are ingested into the human body are transferred, at a rate  $c_i$ , to human vibrios which typically have much higher infectivity/toxicity and could directly lead to human cholera symptoms. Meanwhile, the human vibrios are removed from the human body at a rate  $\xi_i$  due to natural death of the bacteria, shedding of the bacteria to the environment, etc. We assume

$$c_i \ge 0, \quad \xi_i > 0, \quad i = 1, 2, \dots, N.$$

The values of  $c_i$  and  $\xi_i$  could highlight the distinctions among different human individuals. For example, for individuals who are especially vulnerable to cholera (such as young children, old people, or those with poor health), the rate  $c_i$  will be relatively high. In contrast, for individuals who are immune to cholera (due to vaccination, recovery from cholera, etc.) or otherwise are healthy and have a strong immune system, the rate  $c_i$  will be close or equal to 0.

Meanwhile, we assume that for each individual i, a portion  $p_i$  of the removed human vibrios is shed out of the human body and transfer back to the environmental

vibrios. The following equation thus describes the dynamics of the vibrios in the environment:

$$\frac{dB}{dt} = \alpha B \left( 1 - \frac{B}{\kappa} \right) + \sum_{i=1}^{N} p_i \xi_i Z_i - \delta B, \tag{2.3}$$

where the intrinsic growth of the bacteria is modeled by a logistic model with the growth rate  $\alpha$  and carrying capacity  $\kappa$ . The shedding from each human individual contributes to the growth of the bacterial concentration in the environment. In addition,  $\delta$  denotes the natural death rate of the bacteria.

In what follows, we suppose that all model parameters are constants, independent of time, so that Eqs. (2.1)–(2.3) form an autonomous system which allows us to conduct a careful mathematical analysis. We additionally make the following assumptions:

(A1) At any time t, if I(t) > 0, then there exists at least one i such that  $Z_i(t) > 0$ . (A2)  $\delta - \sum_{i=1}^{N} p_i c_i > 0$ .

The condition (A1) sets a positive correlation between the disease prevalence and the within-host dynamics. The condition (A2) implies that in the absence of the intrinsic bacterial growth ( $\alpha = 0$ ), the environmental vibrios would die away eventually.

Below we will analyze the fully coupled, autonomous system that consists of Eqs. (2.1)–(2.3). Brief discussion of decoupled equations based on different time scales is provided in Appendix A.

# ${\bf 2.2.}\ Basic\ reproduction\ number$

It is obvious that there is a unique trivial equilibrium, or disease-free equilibrium (DFE), at

$$S = N, \quad I = B = Z_1 = \dots = Z_N = 0.$$
 (2.4)

We proceed to use the next-generation matrix technique to compute the basic reproduction number,  $R_0$ , for this model. We re-write the equations directly related to the infection as follows:

$$\begin{bmatrix} Z_1' \\ \vdots \\ Z_N' \\ B' \\ I' \end{bmatrix} = \begin{bmatrix} 0 \\ \vdots \\ 0 \\ \alpha B \left( 1 - \frac{B}{\kappa} \right) \\ \beta_H SI + \beta_L SB \end{bmatrix} - \begin{bmatrix} \xi_1 Z_1 - c_1 B \\ \vdots \\ \xi_N Z_N - c_N B \\ \delta B - \sum_{i=1}^N p_i \xi_i Z_i \\ (\mu + \gamma) I \end{bmatrix},$$

where the first part on the right-hand side represents the generation of new infection, and the second part represents the transfer among the disease compartments. The next-generation matrices are given by

$$F = \begin{bmatrix} 0 & \cdots & 0 & 0 & 0 \\ \vdots & \ddots & \vdots & \vdots & \vdots \\ 0 & \cdots & 0 & 0 & 0 \\ 0 & \cdots & 0 & \alpha & 0 \\ 0 & \cdots & 0 & \beta_L N & \beta_H N \end{bmatrix} \equiv \begin{bmatrix} O & O \\ O & E \end{bmatrix}$$

and

$$V = \begin{bmatrix} \xi_1 & \cdots & 0 & -c_1 & 0 \\ \vdots & \ddots & \vdots & \vdots & \vdots \\ 0 & \cdots & \xi_N & -c_N & 0 \\ -p_1 \xi_1 & \cdots & -p_N \xi_N & \delta & 0 \\ 0 & \cdots & 0 & 0 & \mu + \gamma \end{bmatrix} \equiv \begin{bmatrix} A & B \\ C & D \end{bmatrix}.$$

The dimensions of these (non-zero) matrix blocks A, B, C, D and E are  $N \times N, N \times 2, 2 \times N, 2 \times 2$ , and  $2 \times 2$ , respectively.

The basic reproduction number is then determined by the spectral radius of the matrix  $FV^{-1}$ . The inverse of V can be calculated by using the flowing result.

**Lemma 2.1 ([1]).** Consider any square matrix in the form of  $V = \begin{bmatrix} A & B \\ C & D \end{bmatrix}$  where A, B, C and D are matrix blocks, with A and D being square. Then the matrix V is invertible if and only if A and  $D - CA^{-1}B$  are invertible, and  $V^{-1}$  is given by

$$\begin{bmatrix} A & B \\ C & D \end{bmatrix}^{-1} = \begin{bmatrix} A^{-1} + A^{-1}B(D - CA^{-1}B)^{-1}CA^{-1} & -A^{-1}B(D - CA^{-1}B)^{-1} \\ -(D - CA^{-1}B)^{-1}CA^{-1} & (D - CA^{-1}B)^{-1} \end{bmatrix}.$$
(2.5)

Note, however, that E is the only non-zero block in our matrix F. Hence, it is clear that

$$R_0 = \rho(FV^{-1}) = \rho(E(D - CA^{-1}B)^{-1}),$$

where

$$E(D - CA^{-1}B)^{-1} = \begin{bmatrix} \alpha & 0 \\ \beta_L N & \beta_H N \end{bmatrix} \begin{bmatrix} \frac{1}{\delta - \sum_{i=1}^N p_i c_i} & 0 \\ 0 & \frac{1}{\mu + \gamma} \end{bmatrix}$$
$$= \begin{bmatrix} \frac{\alpha}{\delta - \sum_{i=1}^N p_i c_i} & 0 \\ \frac{\beta_L N}{\delta - \sum_{i=1}^N p_i c_i} & \frac{\beta_H N}{\mu + \gamma} \end{bmatrix}.$$

Note that each component in the matrix above is positive based on the assumption (A2). Therefore, we obtain

$$R_0 = \max(R_1, R_2), \tag{2.6}$$

where

$$R_1 = \frac{\alpha}{\delta - \sum_{i=1}^{N} p_i c_i}, \quad R_2 = \frac{\beta_H N}{\mu + \gamma}.$$

**Theorem 2.2.** If  $R_0 \leq 1$ , the DFE is globally asymptotically stable.

**Proof.** Let  $\mathbf{y} = (Z_1, Z_2, \dots, B, I)^T$ . One can verify that

$$\frac{d\mathbf{y}}{dt} \le (F - V)\mathbf{y}.$$

Take

$$\mathbf{u}=(0,\ldots,0,x_1,x_2),$$

where

$$x_1 = (R_2 - R_1)^2 + (R_0 - R_1) \left( \frac{\beta_L N}{\mu + \gamma} - (R_2 - R_1) \right),$$
  
$$x_2 = (R_0 - R_1)(R_2 - R_1).$$

It then follows from the fact  $R_0 = \rho(FV^{-1}) = \rho(V^{-1}F)$  and direct calculation that  $\mathbf{u}$  is a left eigenvector associated with the eigenvalue  $R_0$  of the matrix  $V^{-1}F$ ; i.e.  $\mathbf{u}V^{-1}F = R_0\mathbf{u}$ . Let us consider a Lyapunov function

$$\mathcal{L} = \mathbf{u}V^{-1}\mathbf{y}.$$

Differentiating  $\mathcal{L}$  along the solutions of (2.1)–(2.3), we have

$$\mathcal{L}' = \mathbf{u}V^{-1}\mathbf{y}' \le \mathbf{u}V^{-1}(F - V)\mathbf{y} = (R_0 - 1)\mathbf{u}\mathbf{y}.$$
 (2.7)

Case 1:  $R_0 < 1$ . The equality  $\mathcal{L}' = 0$  implies that  $\mathbf{uy} = 0$ . This leads to  $x_1B + x_2I = 0$ , which yields B = 0,  $I \ge 0$  by noting that  $x_1 > 0$ ,  $x_2 \ge 0$ . If I > 0, then Eqs. (2.1) yield  $I = \frac{\mu}{\beta_H}(R_2 - 1) < \frac{\mu}{\beta_H}(R_0 - 1) < 0$ . The contradiction shows that I = 0, and hence  $\mathbf{y} = 0$ . Therefore, the invariant set on which  $\mathcal{L}' = 0$  contains only one point which is the DFE.

Case 2:  $R_0 = 1$ . The equality  $\mathcal{L}' = 0$  implies that  $\mathbf{y}' = (F - V)\mathbf{y}$ , which yields B = 0 and S = N. Thus,  $\mathbf{y} = 0$  holds again.

Therefore, in either case, the largest invariant set on which  $\mathcal{L}' = 0$  consists of the singleton  $X_0 = (N, 0, \dots, 0)$ . By LaSalle's Invariance Principle, the DFE is globally asymptotically stable.

## 2.3. Non-trivial equilibria

We denote a non-trivial equilibrium by

$$X^* = (B^*, S^*, I^*, Z_1^*, Z_2^*, \dots, Z_N^*),$$

where, for convenience of algebraic manipulation, we put  $B^*$  as the first component. At  $X^*$ , we have

$$\mu N - \beta_H S^* I^* - \beta_L S^* B^* - \mu S^* = 0,$$

$$\beta_H S^* I^* + \beta_L S^* B^* - (\gamma + \mu) I^* = 0,$$

$$\alpha B^* \left( 1 - \frac{B^*}{\kappa} \right) + \sum_{i=1}^N p_i \xi_i Z_i^* - \delta B^* = 0,$$

$$c_i B^* - \xi_i Z_i^* = 0.$$
(2.8)

From the last two equations in (2.8) we obtain

$$\left\{ \left[ \sum_{i=1}^{N} p_i c_i + \alpha - \delta \right] - \frac{\alpha}{\kappa} B^* \right\} B^* = 0.$$
 (2.9)

The solution of Eq. (2.9) is given by  $B^* = 0$ , or

$$B^* = \frac{\kappa}{\alpha} \left[ \sum_{i=1}^{N} p_i c_i + \alpha - \delta \right] = \kappa \left( 1 - \frac{1}{R_1} \right), \tag{2.10}$$

where  $R_1$  is defined in (2.6). It is clear to see that  $B^* > 0$  if and only if  $R_1 > 1$ . Note that this result is consistent with the findings based on the separation of scales (see Appendix A).

When  $R_1 \leq 1$ , the only non-negative solution for  $B^*$  is  $B^* = 0$ . Consequently,  $Z_i^* = 0$  for  $1 \leq i \leq N$ . Meanwhile, the first two equations in (2.8) yield

$$\mu N - \beta_H S^* I^* - \mu S^* = 0,$$
  

$$\beta_H S^* I^* - (\gamma + \mu) I^* = 0.$$
(2.11)

In addition to the trivial solution  $(I^*, S^*) = (0, N)$ , there is a unique non-trivial solution given as

$$(I^*, S^*) = \left(\frac{\mu}{\beta_H}(R_2 - 1), \frac{\gamma + \mu}{\beta_H}\right),$$
 (2.12)

where  $R_2$  is defined in (2.6). Obviously  $I^* > 0$  if and only if  $R_2 > 1$ . In this case we obtain a non-trivial boundary equilibrium.

When  $R_1 > 1$ , then  $B^* > 0$ . The last equation in (2.8) yields

$$Z_i^* = \frac{c_i B^*}{\xi_i}, \quad i = 1, 2, \dots, N.$$

Meanwhile, the second equation of (2.8) yields

$$S^* = \frac{(\gamma + \mu)I^*}{\beta_H I^* + \beta_L B^*} > 0$$

provided that  $I^* > 0$ . Adding the first two equations in (2.8), we obtain

$$\mu N = \mu S^* + (\mu + \gamma)I^*$$

which yields

$$S^* = N - \left(1 + \frac{\gamma}{\mu}\right)I^*.$$

Substitute this into the second equation of (2.8) to obtain

$$\beta_H \left( 1 + \frac{\gamma}{\mu} \right) (I^*)^2 + \left[ (\gamma + \mu) \left( 1 + \frac{\beta_L}{\mu} B^* \right) - N \beta_H \right] I^* - N \beta_L B^* = 0.$$
 (2.13)

Clearly, when  $B^* > 0$ , there is only one positive root,  $I^*$ , for Eq. (2.13). In this case we have a unique endemic equilibrium.

Summarizing the results above, we have the following theorem.

**Theorem 2.3.** The system has a non-trivial, non-negative equilibrium if and only if  $R_0 > 1$ . Specifically:

- (1) If  $R_1 \leq 1$  and  $R_2 > 1$ , then there is a unique boundary equilibrium  $X_1^*$  represented by  $I^* = \frac{\mu}{\beta_H}(R_2 1)$ ,  $S^* = \frac{\gamma + \mu}{\beta_H}$ , and  $B^* = Z_1^* = \cdots = Z_N^* = 0$ .
- (2) If  $R_1 > 1$ , then there is a unique endemic equilibrium  $X_2^*$  represented by  $B^* = \kappa(1 \frac{1}{R_1})$ ,  $Z_i^* = \frac{c_i B^*}{\xi_i}$   $(1 \le i \le N)$ ,  $I^* > 0$ , and  $S^* = \frac{(\gamma + \mu)I^*}{\beta_H I^* + \beta_L B^*}$ .

Note that the boundary equilibrium  $X_1^*$  means that the between-host dynamics are totally decoupled from the environment and the within-host dynamics; that is, the environmental pathogen concentration and the within-host pathogen load have no impact on the disease prevalence. This is unreasonable for a water-borne disease such as cholera. Indeed, our assumption (A1) excludes the boundary equilibrium

 $X_1^*$ . Hence, in what follows we will focus our attention on the endemic equilibrium  $X_2^*$ .

The Jacobian at the endemic equilibrium is then given by

$$J(X_2^*) = \begin{bmatrix} \alpha - \delta - \frac{2\alpha}{\kappa} B^* & 0 & 0 & p_1 \xi_1 & p_2 \xi_2 & \cdots & p_N \xi_N \\ -\beta_L S^* & -(\beta_H I^* + \beta_L B^* + \mu) & -\beta_H S^* & 0 & 0 & \cdots & 0 \\ \beta_L S^* & \beta_H I^* + \beta_L B^* & \beta_H S^* - (\gamma + \mu) & 0 & 0 & \cdots & 0 \\ c_1 & 0 & 0 & -\xi_1 & 0 & \cdots & 0 \\ c_2 & 0 & 0 & 0 & -\xi_2 & \cdots & 0 \\ \vdots & \vdots & \vdots & \vdots & \vdots & \vdots & \ddots & \vdots \\ c_N & 0 & 0 & 0 & 0 & 0 & \cdots & -\xi_N \end{bmatrix}.$$

After some algebraic manipulation, the characteristic polynomial associated with  $J(X_2^*)$  can be found as

$$\det(\lambda I - J(X_2^*)) = \Gamma_1(\lambda)\Gamma_2(\lambda), \tag{2.14}$$

where

$$\Gamma_{1}(\lambda) = \det \begin{bmatrix} \lambda + \beta_{H}I^{*} + \beta_{L}B^{*} + \mu & \beta_{H}S^{*} \\ -(\beta_{H}I^{*} + \beta_{L}B^{*}) & \lambda - \beta_{H}S^{*} + \gamma + \mu \end{bmatrix}$$
$$= \lambda^{2} + (\beta_{H}I^{*} + \beta_{L}B^{*} - \beta_{H}S^{*} + \gamma + 2\mu)\lambda$$
$$+ [(\beta_{H}I^{*} + \beta_{L}B^{*} + \mu)(\gamma + \mu) - \mu\beta_{H}S^{*}],$$

and

$$\Gamma_2(\lambda) = \left(\lambda + \delta - \alpha + \frac{2\alpha}{\kappa} B^*\right) H(\lambda) + p_1 \xi_1 c_1 \frac{H(\lambda)}{\lambda + \xi_1} + p_2 \xi_2 c_2 \frac{H(\lambda)}{\lambda + \xi_2} + \dots + p_N \xi_N c_N \frac{H(\lambda)}{\lambda + \xi_N}$$

with

$$H(\lambda) = (\lambda + \xi_1)(\lambda + \xi_2) \cdots (\lambda + \xi_N).$$

Using the second equation in (2.8), one can easily see that  $\beta_H S^* < \gamma + \mu$ , and thus each coefficient of  $\Gamma_1(\lambda)$  is positive. Consequently, the two roots of  $\Gamma_1(\lambda)$  both have negative real parts. Meanwhile, note that when  $R_1 > 1$ , we have

$$\delta - \alpha + \frac{2\alpha}{\kappa} B^* = 2\sum_{k=1}^{N} p_k c_k + \alpha - \delta > \sum_{k=1}^{N} p_k c_k > 0.$$
 (2.15)

Thus, each coefficient in the polynomial  $\Gamma_2(\lambda)$  is positive.

**Theorem 2.4.** The endemic equilibrium  $X_2^*$  is locally asymptotically stable.

**Proof.** We only need to show that each root of  $\Gamma_2(\lambda)$  has a negative real part. Let  $\rho > 0$  be a positive number, to be determined, and

$$\gamma_{\rho} = \left\{ z \, | \, z = \rho e^{i\theta}, \frac{\pi}{2} \le \theta \le \frac{3\pi}{2} \right\} \cup \{ z \, | \, z = yi, -\rho \le y \le \rho \}, \text{ where } i^2 = -1,$$

be a simple closed contour. Denote  $F(\lambda)=(\lambda+A)H(\lambda)$ , where  $A=\delta-\alpha+\frac{2\alpha}{\kappa}B^*>0$  by Eq. (2.15). Then  $\Gamma_2(\lambda)=F(\lambda)+H(\lambda)\sum_{k=1}^N\frac{p_kc_k\xi_k}{\lambda+\xi_k}$ . Obviously,  $\Gamma_2(\lambda)$  and  $F(\lambda)$  are both analytic inside and on  $\gamma$ . We will show that

$$|\Gamma_2(\lambda) - F(\lambda)| < |F(\lambda)| \quad \text{on } \gamma_{\rho}.$$
 (2.16)

Then, by Rouché Theorem [7], we know that  $\Gamma_2(\lambda)$  and  $F(\lambda)$  must have the same number of zeros, counting multiplicities, inside  $\gamma_{\rho}$ , which is on the left half complex plane.

(i) If 
$$\lambda = yi$$
,  $-\rho \le y \le \rho$ , then

$$|\Gamma_{2}(yi) - F(yi)| = \left| H(yi) \sum_{k=1}^{N} \frac{p_{k} c_{k} \xi_{k}}{yi + \xi_{k}} \right|$$

$$\leq |H(yi)| \sum_{k=1}^{N} \left| \frac{p_{k} c_{k} \xi_{k}}{\sqrt{y^{2} + \xi_{k}^{2}}} \right|$$

$$\leq |H(yi)| \sum_{k=1}^{N} p_{k} c_{k} < |H(yi)| A \quad \text{by (2.15)}$$

$$\leq |H(yi)| |A + yi| = |F(yi)|.$$

(ii) If 
$$z = \rho e^{i\theta}$$
,  $\frac{\pi}{2} \le \theta \le \frac{3\pi}{2}$ ,  $\rho > 0$ , then

$$|\Gamma_2(\rho e^{i\theta}) - F(\rho e^{i\theta})| = \left| H(\rho e^{i\theta}) \sum_{k=1}^N \frac{p_k c_k \xi_k}{\rho e^{i\theta} + \xi_k} \right| \le |H(\rho e^{i\theta})| \sum_{k=1}^N \frac{p_k c_k \xi_k}{|\rho e^{i\theta} + \xi_k|}.$$

Notice that  $\lim_{\rho\to\infty}\sum_{k=1}^N\frac{p_kc_k\xi_k}{|\rho e^{i\theta}+\xi_k|}=0$  and  $\lim_{\rho\to\infty}|\rho e^{i\theta}+A|=+\infty$ , hence we can choose  $\rho>\max\{A,\xi_1,\ldots,\xi_N\}$  such that  $\sum_{k=1}^N\frac{p_kc_k\xi_k}{|\rho e^{i\theta}+\xi_k|}<|\rho e^{i\theta}+A|$ . Thus, (2.16) holds for some  $\rho>0$ . Since all N+1 zeros of  $F(\lambda)$  are inside  $\gamma_\rho$ , we obtain that all N+1 zeros of  $\Gamma_2(\lambda)$  are inside  $\gamma_\rho$ ; i.e. the real part of every zero of  $\Gamma_2(\lambda)$  is negative. Therefore,  $X_2^*$  is locally stable.

In contrast, the global asymptotic stability of an endemic equilibrium is usually difficult to establish, when the dimension of the system is high. The proof of such global stability, if available, normally comes with additional conditions on the model [8, 17]. In our case, we have the following result.

**Theorem 2.5.** The endemic equilibrium  $X_2^*$  is globally asymptotically stable if  $2 + \frac{B}{B^*} \le \frac{I}{I^*} + \frac{S^*}{S} + \frac{SI^*B}{S^*IB^*}$ .

**Proof.** We consider a Lyapunov function

$$\mathcal{L} = a_1 D_1 + a_2 D_2 + a_3 D_3 + \sum_{i=1}^{N} A_i E_i,$$

where

$$D_1 = \left(S - S^* - S^* \ln\left(\frac{S}{S^*}\right)\right), \quad D_2 = \left(I - I^* - I^* \ln\left(\frac{I}{I^*}\right)\right),$$

$$D_3 = \left(B - B^* - B^* \ln\left(\frac{B}{B^*}\right)\right), \quad E_i = \left(Z_i - Z_i^* - Z_i^* \ln\left(\frac{Z_i}{Z_i^*}\right)\right),$$

$$i = 1, 2, \dots, N,$$

and  $a_j > 0$  (j = 1, 2, 3, 4),  $A_i > 0$  (i = 1, 2, ..., N) are constants to be determined. It is easy to verify that  $\mathcal{L} \geq 0$  for all positive  $S, I, B, Z_i$  (i = 1, 2, ..., N), and  $\mathcal{L} = 0$  if and only if  $(S, I, B, Z_1, ..., Z_N) = X_2^*$ . Differentiating  $\mathcal{L}$  along the vector field of the system, we obtain

$$\begin{split} \mathcal{L}' &= a_1 D_1' + a_1 D_2' + a_3 D_3' + \sum_{i=1}^{N} A_i E_i' \\ &= a_1 \left( 1 - \frac{S^*}{S} \right) S' + a_2 \left( 1 - \frac{I^*}{I} \right) I' + a_3 \left( 1 - \frac{B^*}{B} \right) B' + \sum_{i=1}^{N} A_i \left( 1 - \frac{Z_i^*}{Z_i} \right) Z_i' \\ &= -a_1 \mu \frac{(S - S^*)^2}{S} + a_1 \beta_H S^* I^* \left( 1 - \frac{S^*}{S} + \frac{I}{I^*} - \frac{SI}{S^* I^*} \right) \\ &+ \frac{\beta_L}{\beta_H} \left( \frac{B^* + B}{I^*} - \frac{SB}{S^* I^*} - \frac{S^* B^*}{SI^*} \right) \right) + a_2 \beta_H S^* I^* \left( 1 - \frac{I}{I^*} - \frac{S}{S^*} + \frac{SI}{S^* I^*} \right) \\ &+ \frac{\beta_L}{\beta_H} \left( \frac{B^*}{I^*} - \frac{SB}{S^* I} + \frac{SB}{S^* I^*} - \frac{IB^*}{I^{*2}} \right) \right) - a_3 \frac{\alpha}{\kappa} (B - B^*)^2 \\ &+ a_3 \sum_{i=1}^{N} p_i \xi_i Z_i^* \left( 1 - \frac{B}{B^*} + \frac{Z_i}{Z_i^*} - \frac{Z_i B^*}{Z_i^* B} \right) + \sum_{i=1}^{N} A_i \xi_i Z_i^* \left( 1 - \frac{Z_i}{Z_i^*} + \frac{B}{B^*} - \frac{Z_i^* B}{Z_i B^*} \right) \\ &\leq a_1 \beta_H S^* I^* \left( 1 - \frac{S^*}{S} + \frac{I}{I^*} - \frac{SI}{S^* I^*} + \frac{\beta_L}{\beta_H} \left( \frac{B^* + B}{I^*} - \frac{SB}{S^* I^*} - \frac{S^* B^*}{SI^*} \right) \right) \\ &+ a_2 \beta_H S^* I^* \left( 1 - \frac{I}{I^*} - \frac{S}{S^*} + \frac{SI}{S^* I^*} + \frac{\beta_L}{\beta_H} \left( \frac{B^*}{I^*} - \frac{SB}{S^* I} + \frac{SB}{S^* I^*} - \frac{IB^*}{I^{*2}} \right) \right) \\ &+ a_3 \sum_{i=1}^{N} p_i \xi_i Z_i^* \left( 1 - \frac{B}{B^*} + \frac{Z_i}{Z_i^*} - \frac{Z_i B^*}{Z_i^* B} \right) + \sum_{i=1}^{N} A_i \xi_i Z_i^* \left( 1 - \frac{Z_i}{Z_i^*} + \frac{B}{B^*} - \frac{Z_i^* B}{Z_i B^*} \right) \right) \\ &+ a_3 \sum_{i=1}^{N} p_i \xi_i Z_i^* \left( 1 - \frac{B}{B^*} + \frac{Z_i}{Z_i^*} - \frac{Z_i B^*}{Z_i^* B} \right) + \sum_{i=1}^{N} A_i \xi_i Z_i^* \left( 1 - \frac{Z_i}{Z_i^*} + \frac{B}{B^*} - \frac{Z_i^* B}{Z_i B^*} \right) \right) \\ &+ a_3 \sum_{i=1}^{N} p_i \xi_i Z_i^* \left( 1 - \frac{B}{B^*} + \frac{Z_i}{Z_i^*} - \frac{Z_i B^*}{Z_i^* B} \right) + \sum_{i=1}^{N} A_i \xi_i Z_i^* \left( 1 - \frac{Z_i}{Z_i^*} + \frac{B}{B^*} - \frac{Z_i^* B}{Z_i B^*} \right) \\ &+ a_3 \sum_{i=1}^{N} p_i \xi_i Z_i^* \left( 1 - \frac{B}{B^*} + \frac{Z_i}{Z_i^*} - \frac{Z_i B^*}{Z_i^* B} \right) + \sum_{i=1}^{N} A_i \xi_i Z_i^* \left( 1 - \frac{Z_i}{Z_i^*} + \frac{B}{B^*} - \frac{Z_i^* B}{Z_i B^*} \right) \right) \\ &+ a_3 \sum_{i=1}^{N} p_i \xi_i Z_i^* \left( 1 - \frac{B}{B^*} + \frac{Z_i}{Z_i^*} - \frac{Z_i B^*}{Z_i^* B} \right) + \sum_{i=1}^{N} A_i \xi_i Z_i^* \left( 1 - \frac{Z_i}{Z_i^*} + \frac{B}{B^*} - \frac{Z_i^* B}{Z_i B^*} \right) \right) \\ &+ a_3 \sum_{i=1}^{N} p_i \xi_i Z_i^* \left( 1 - \frac{B}{B^*} + \frac{Z_i}{Z_i^*} - \frac{Z_i B^*}{Z_i^* B} \right) + \sum_{i=1}^{N}$$

Take  $a_1 = a_2 = a_3 = 1$  and  $A_i = p_i \ (i = 1, 2, ..., N)$ . Then

$$\mathcal{L}' \leq \beta_H S^* I^* \left( 2 - \frac{S^*}{S} - \frac{S}{S^*} \right) + \sum_{i=1}^N p_i \xi_i Z_i^* \left( 2 - \frac{Z_i B^*}{Z_i^* B} - \frac{Z_i^* B}{Z_i B^*} \right) + \beta_L S^* B^* \left( 2 + \frac{B}{B^*} - \frac{I}{I^*} - \frac{S^*}{S} - \frac{SI^* B}{S^* I B^*} \right).$$

By our assumption, the last term is non-positive. Thus,  $\mathcal{L}' \leq 0$ . Moreover,  $\mathcal{L}' = 0$  if and only if  $S = S^*$ ,  $I = I^*$ ,  $B = B^*$ . Therefore, the largest invariant set for which  $\mathcal{L}' = 0$  contains only  $X_2^*$ . By LaSalle's Invariance Principle,  $X_2^*$  is globally asymptotically stable.

### 3. Numerical Results

In this section, we conduct numerical simulation to our proposed multi-scale cholera model, both to verify our analytical results and to explore scenarios that are not covered in our analysis. To make distinction among hosts, we label all the individuals by integers from 1 to N; thus, each individual is assigned a unique numeric "ID" that belongs to the set  $\{1, 2, \ldots, N\}$ .

## 3.1. Constant parameters

We first consider the case where each parameter is fixed as a constant. Our mathematical analysis is concerned with this scenario and Theorems 2.2 and 2.5 predict the global stabilities of the DFE and the endemic equilibrium, respectively.

In our numerical tests, we use the base values of the model parameters provided in Table 1. Meanwhile, we set the initial conditions as follows:

$$I(0) = J$$
,  $R(0) = 0$ ,  $S(0) = N - I(0) - R(0)$ ,  
 $B(0) = 10^4 \text{ cells/ml}$ ,  $Z_i(0) = 0$ 

for  $1 \leq i \leq N$  and some positive integer  $J \geq 1$ . For those individuals who are initially infected,  $c_i \neq 0$ , for  $1 \leq i \leq J$ . Here, for simplicity, we assume that the individuals labeled with  $1 \leq i \leq J$  are initially infected. Thus, we set  $c_i > 0$  for  $1 \leq i \leq J$ , and  $c_i = 0$  for  $J + 1 \leq i \leq N$ .

Figure 1 illustrates that when  $R_0 < 1$ , the DFE is globally asymptotically stable. In contrast, Fig. 2 shows that when  $R_0 > 1$ , the endemic equilibrium is globally asymptotically stable. In these two cases, we simply set  $c_i = 2$  for i = 1, 2, ..., J. The results are consistent with the analytical predictions in Theorems 2.2 and 2.5. Additionally, to examine the specific dynamical behavior of the human vibrios within different hosts, we set  $c_i = 0.04 * i$  for  $1 \le i \le J$ , and  $c_i = 0$  for i > J, with J = 10. Other parameter values remain the same. We then plot the time evolution of  $Z_i(t)$  for a few typical (initially infected) individuals in Fig. 3. We see that each curve starts from 0 and increases quickly during the first few hours, showing the fast

Parameter	Definition	Value	References
N	Total number of human individuals	10,000 p	Assumed
$\mu$	Natural human birth/death rate	$(15,878 \mathrm{d})^{-1}$	[11]
$\beta_H$	Direct transmission rate	$1.57 \times 10^{-5} \mathrm{d}^{-1}$	[11]
$eta_L$	Indirect transmission rate	$1.1 \times 10^{-8} \mathrm{p}^{-1} \mathrm{d}^{-1}$	[11]
$\gamma$	Recovery rate	$0.2{\rm d}^{-1}$	[10]
$c_i$	Transfer rate from environmental vibrios to human vibrios	Varied	
$\xi_i$	Removal rate of human vibrios	$10{\rm d}^{-1}$	Assumed
$\alpha$	Bacterial growth rate	$0.1{\rm d}^{-1}$	Assumed
$\kappa$	Bacterial carrying capacity	$10^6  \mathrm{cells \cdot ml^{-1}}$	[22]
$p_i$	Portion of human vibrios back to environmental vibrios	10%	Assumed
δ	Death rate of environmental vibrios	$(30  d)^{-1}$	[10]

Table 1. Model parameters and their values (p = person, d = day).

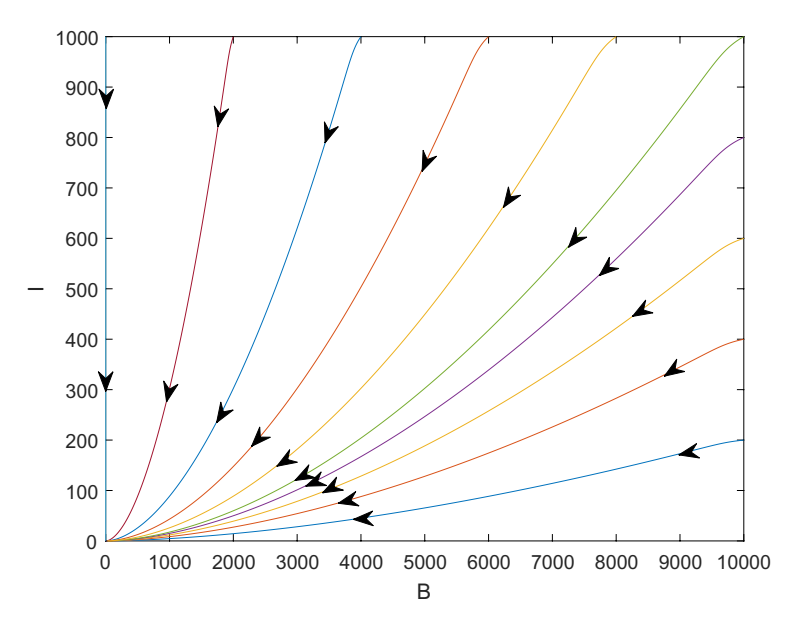


Fig. 1. A typical phase portrait for I vs. B when  $R_0 < 1$ . Each curve starts with a different initial condition, and all these curves converge to the DFE at (B, I) = (0, 0), illustrating that the DFE is globally asymptotically stable when  $R_0 < 1$ .

increase of the pathogen load within the human body upon infection. Among these curves,  $Z_{10}(t)$  and  $Z_1(t)$  attain the highest and lowest levels, due to that  $c_{10}$  and  $c_1$  have the largest and smallest values, respectively. Moreover, each curve approaches a positive steady state over time, another evidence of the stability of the endemic equilibrium.

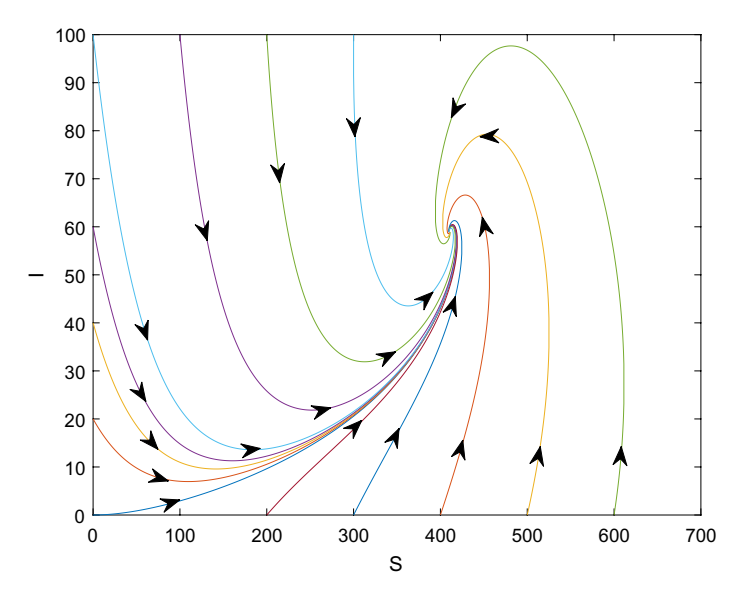


Fig. 2. A typical phase portrait for I vs. S when  $R_0 > 1$ . Each curve starts with a different initial condition, and all these orbits approach the endemic equilibrium at  $(S, I) \approx (410, 59)$ , illustrating that the endemic equilibrium is globally asymptotically stable when  $R_0 > 1$ .

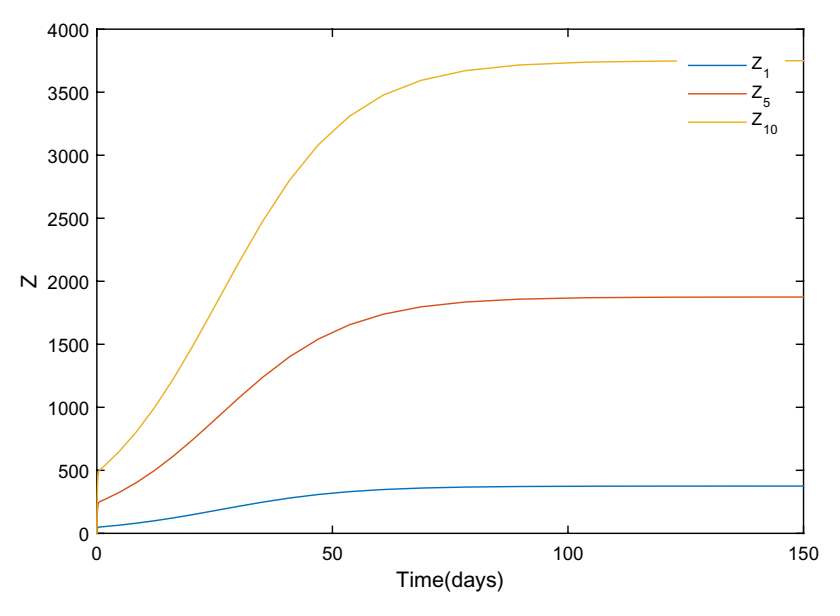


Fig. 3.  $Z_i$  vs. time for i=1,5,10. Each curve starts with  $Z_i(0)=0$  and increases over time, approaching a steady state. The value of  $c_i$  increases with i for  $1 \le i \le 10$ , and so  $Z_{10}(t)$  attains the highest level among these curves.

## 3.2. Time-dependent parameters

Our mathematical analysis presented in Sec. 2 requires that each parameter remains fixed (or, "static"), independent of time, so as to investigate the essential dynamics concerned with equilibria and stabilities. Nevertheless, our modeling framework allows the parameters, particularly  $c_i$ 's, to be time-dependent. In order to better understand the interaction between the within-host and between-host dynamics, we utilize numerical means to explore an "adaptive" modeling approach, with a focus on the "dynamic" changes of the parameters  $c_i$ 's to reflect a stronger correlation between the disease prevalence and the within-host pathogen load. Specifically, we will assume that at any time t,

- (H1) if the *i*th individual  $(1 \le i \le N)$  belongs to the infected class I (i.e. already infected), then  $c_i(t) > 0$ ;
- (H2) if the *i*th individual  $(1 \le i \le N)$  belongs to the susceptible class S or recovered class R (i.e. not infected at the time), then  $c_i(t) = 0$ .

For simplicity, we also assume that throughout the process, each  $c_i$  will switch between 0 and a constant C > 0, depending on the classification of the *i*th individual (infected, susceptible, or recovered). Additionally, we neglect the natural human birth and death; i.e.  $\mu = 0$ .

As before, we suppose that there are J infected hosts initially, for individuals labeled with  $1 \leq i \leq J$ . We then set  $c_1(0) = \cdots = c_J(0) = C$ , and  $c_{J+1}(0) = \cdots = c_N(0) = 0$ . Other parameters and initial conditions remain the same as in the static case. In addition, for  $n = 1, 2, 3, \ldots$ , we let  $I_n$  and  $R_n$  denote the largest integers not exceeding I(n) and R(n), respectively, at day n. The values of  $I_n$  and  $R_n$  are used to group the within-host compartments: for  $i \leq R_n$ , the individual i belongs to the recovered class; for  $R_n < i \leq R_n + I_n$ , the individual i belongs to the susceptible class. For example, the recovery period is five days in our setting; i.e.  $\gamma = 0.2$  per day. Then at n = 5 the individuals  $1 \leq i \leq J$  (who are initially infected) are moved to the recovered class; meanwhile, other individuals may have been infected during this period and they are labeled with  $i = J + 1, J + 2, \ldots$  in an increasing order.

We then run the numerical simulation to the ODE system using a small time step (e.g.  $\Delta t = 0.01 \,\text{day}$ ) and update  $I_n$  and  $R_n$  once for each day; i.e. at  $n = 1, 2, 3, \ldots$  Meanwhile, we update the values of  $c_i$ 's accordingly; that is,  $c_i(n) = C$  for  $R_n < i \le R_n + I_n$ , and  $c_i(n) = 0$  for  $i \le R_n$  or  $R_n + I_n < i \le N$ .

Figures 4–6 show the results for a small host population N=100, where we set J=1; i.e. initially there is only one infected individual associated with i=1. In particular, we plot the human vibrio concentrations in Fig. 4 that show the variations of  $Z_i(t)$  with respect to the host ID  $(1 \le i \le N)$  and time (t). Since the recovery rate is  $\gamma = 0.2$  per day, each infected individual stays in the infected class (with positive  $Z_i$ ) for five days and then recovers. From the figure, we can clearly see that for each host ID  $1 \le i \le N$ , there is only a short period (about several days)

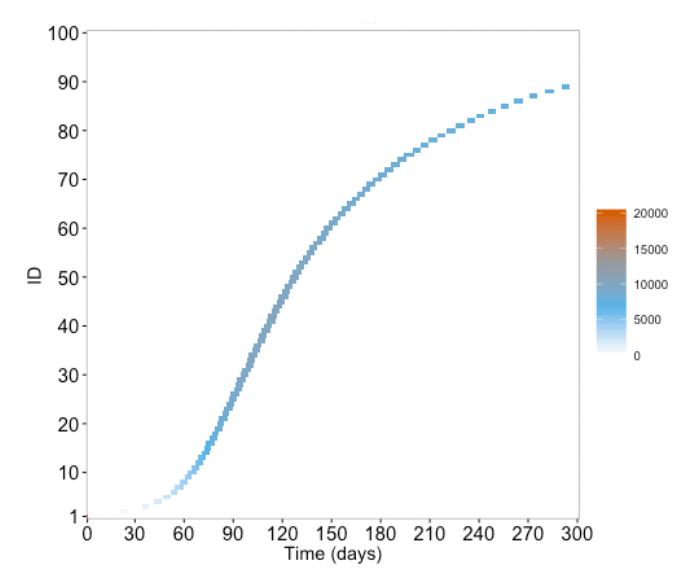


Fig. 4. (Color online) Variations of  $Z_i(t)$  with respect to the host ID  $(1 \le i \le N)$  and time (t). Here N = 100 and J = 1.

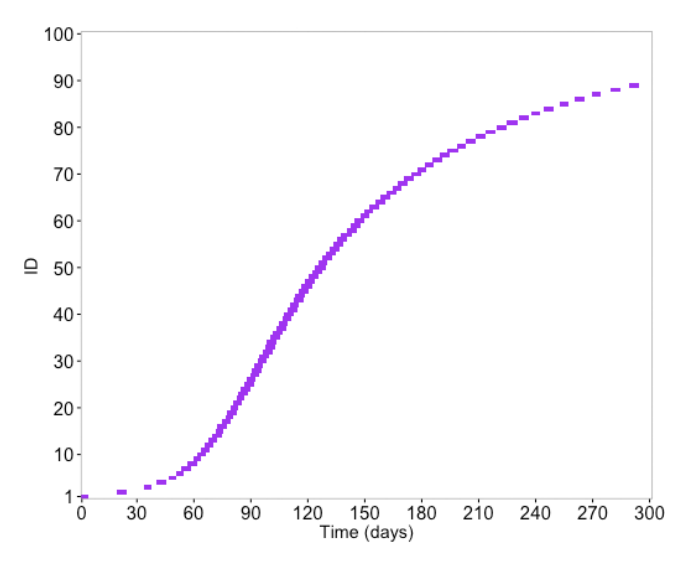


Fig. 5. Variations of  $c_i(t)$  with respect to the host ID  $(1 \le i \le N)$  and time (t). The color (purple) indicates  $c_i(t) > 0$ . Here N = 100 and J = 1.

in which  $Z_i(t)$  is non-zero, indicating that the human vibrios are short-lived [10]. Starting with the host ID i=1, the infection sweeps the entire population, with those host IDs associated with higher numeric values getting infected at later times. At any single time, multiple individuals are in the infected class with non-zero  $Z_i$ 's. In addition, the level of (non-zero)  $Z_i$ 's remains relatively low during the initial

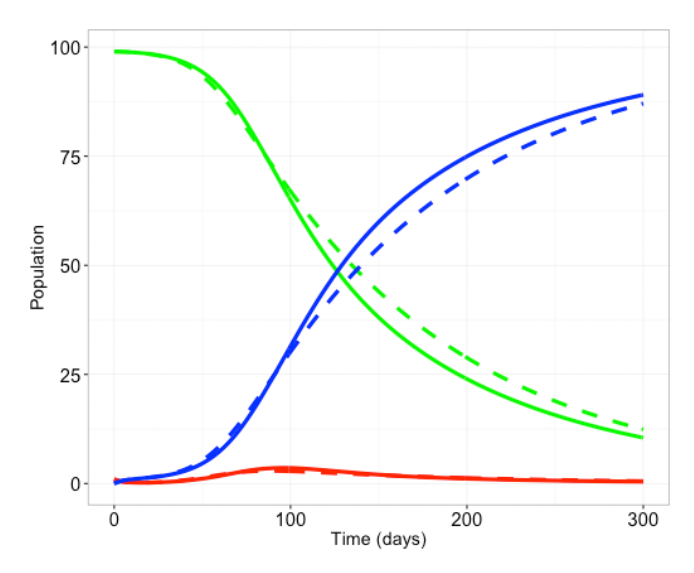


Fig. 6. Comparison between the dynamic case (solid line) and the static case (dashed line) with N = 100 and J = 1. Green: susceptible class; Red: infected class; Blue: recovered class.

period (0 < t < 30 days), but it keeps increasing with time. When t > 60 days, the values of all non-zero  $Z_i$ 's appear to stabilize around 5,000 cells/ml.

Figure 5 shows the variations of  $c_i(t)$  with respect to the host ID  $(1 \le i \le N)$  and time (t), where the color (purple) indicates that  $c_i(t) = C > 0$  and, otherwise,  $c_i(t) = 0$ . We see that the pattern is consistent with that in Fig. 4.

Figure 6 shows the comparison between the dynamic case (with time-dependent parameters) and the static case (with fixed parameters) for the evolution of host populations, under the same initial setting. We see that while the infection curves in the two scenarios well match each other, there are slight differences in the variation of the susceptible and recovered populations under these two settings.

Figures 7–9 show the results for a relatively large host population N=10,000, where we assume J=10; i.e. initially there are 10 infected individuals associated with  $1 \le i \le 10$ . We note that the epidemic in this scenario is much shorter (around 80 days) compared to that when N=100 (greater than 300 days). We again plot the variations of  $Z_i(t)$  and  $c_i(t)$  with respect to host IDs and time, in Figs. 7 and 8, respectively. Comparing with Fig. 4, we see that, in Fig. 7, during the period between the 52nd and 60th days, the non-zero values of  $Z_i(t)$ 's reach a very high level (up to  $6 \times 10^5$ ). Meanwhile, it can be observed that at any day during this period, there can be as many as a few thousands of infected individuals, reflected by the long vertical bars in the figure. Our results indicate that this period represents the peak of the disease outbreak, and that the epidemic peak coincides in time with the peak values of the within-host vibrio concentrations, demonstrating a strong correlation between the disease transmission at the population level and the

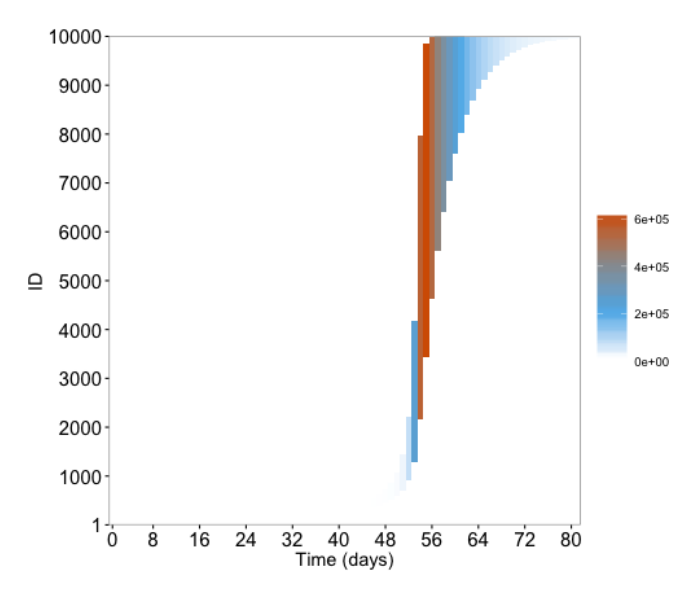


Fig. 7. (Color online) Variations of  $Z_i(t)$  with respect to the host ID  $(1 \le i \le N)$  and time (t). Here  $N = 10{,}000$  and J = 10.

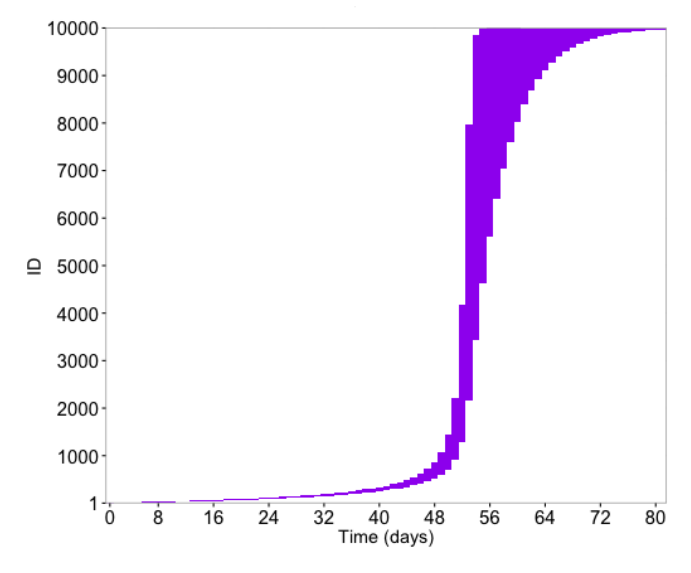


Fig. 8. (Color online) Variations of  $c_i(t)$  with respect to the host ID  $(1 \le i \le N)$  and time (t). The color (purple) indicates  $c_i(t) > 0$ . Here N = 10,000 and J = 10.

pathogen load at the individual level. Afterwards, the values of the non-zero  $Z_i(t)$ 's decrease with time, and the number of infected individuals at a single day also decreases, showing that the epidemic is slowed down (and eventually gone). The plot of the variation of  $c_i(t)$  in Fig. 8 shows a pattern consistent with that in Fig. 7.

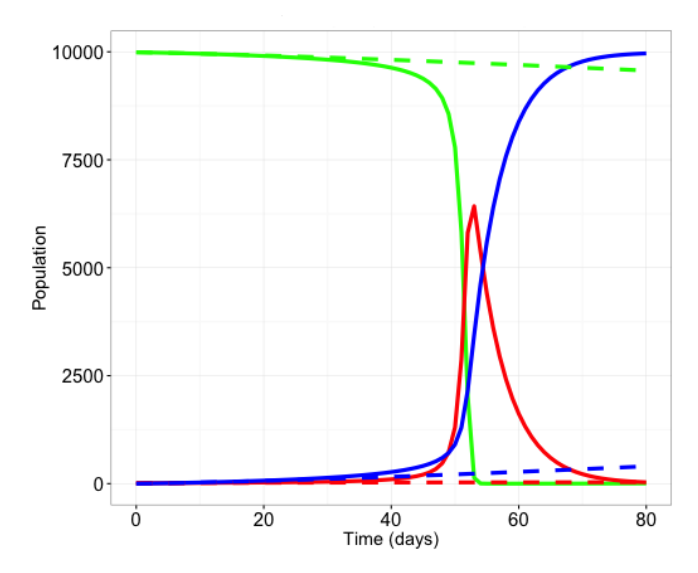


Fig. 9. Comparison between the dynamic case (solid line) and the static case (dashed line) with N = 10,000 and J = 10. Green: susceptible class; Red: infected class; Blue: recovered class.

Figure 9 again compares the dynamic and static cases for the evolution of host populations, under the same initial setting. Unlike the result in Fig. 6, now we see large discrepancies between these two scenarios, especially the very high epidemic peak in the dynamic case vs. the very low peak in the static case. As the dynamic model provides a stronger connection for the between-host and within-host dynamics and is potentially more realistic, this result implies that when the population is relatively large, using the static model (with fixed parameters) might yield very inaccurate prediction.

#### 4. Discussion

We have presented a new deterministic modeling framework to link the betweenhost and within-host dynamics of cholera. The major innovation of our work is the representation of each individual host in a separate manner which allows natural incorporation of host heterogeneities into the within-host dynamics, yet keeping the model mathematically and computationally tractable.

We have focused our attention on the case where each model parameter is a constant independent of time. For this autonomous model, we are able to conduct a detailed mathematical analysis. We have shown the existence and uniqueness of the DFE and the endemic equilibrium, and established their stabilities using threshold conditions based on the basic reproduction number. In particular, a result from complex analysis (the Rouché Theorem) helps us to prove the local stability of the endemic equilibrium, and the use of a Lyapunov function allows us to establish its

global stability under some additional constraint. Our numerical simulation results are consistent with these analytical findings.

In addition, we have numerically explored our model with time-dependent within-host parameters, where the transfer rates from environmental vibrios to human vibrios associated with each individual host change with time, depending on whether or not the individual is infected. This non-autonomous model strengthens the link between the within-host and between-host dynamics by emphasizing a feedback mechanism: the disease transmission at the population (or, macroscopic) level impacts the pathogen load at the individual (or, microscopic) level, whereas the variation of the pathogen concentrations inside the human body shapes the classifications of hosts (susceptible, infected, and recovered) and their interactions outside the human body. This study could be a starting point for establishing a comprehensive, adaptive modeling framework for cholera with a strong and consistent connection between the within-host and between-host dynamics.

Although our current model allows the incorporation of heterogeneities from different host individuals, the characterization of the within-host dynamics for each individual is still simple, represented by a single equation for each. Our future work will seek to improve it by incorporating the interactions among the vibrios, choleratoxin phages, and the immune response, so as to gain deeper understanding on the complex processes of pathogen evolution inside the human body. We will again combine mathematical analysis and numerical simulation in such research tasks.

### Acknowledgments

F. Bao was partially supported by the National Science Foundation under Grant No. 1720222. J. Wang was partially supported by the National Science Foundation under Grant Nos. 1412826 and 1557739. The authors are grateful to the two anonymous referees for their valuable comments that have improved this paper.

## Appendix A. Separation of Scales

A simplified model analysis for the system (2.1)–(2.3) can be conducted by separating the time scales, since the within-host dynamics are on a fast scale and typically range from several hours to a few days, whereas the between-host dynamics and the evolution of the environmental bacterial densities are on a slow scale and normally take place in months and years. Thus, we may treat the slow variable B as a constant in the fast-scale (within-host) model (2.3) to obtain

$$Z_{i}(t) = \frac{c_{i}B}{\xi_{i}} + \left[Z_{i}(0) - \frac{c_{i}B}{\xi_{i}}\right]e^{-\xi_{i}t}.$$
 (A.1)

Note that  $\xi_i > 0$  for  $1 \le i \le N$ . Equation (A.1) shows that for each fixed B > 0,  $Z_i$  would exponentially converge to its equilibrium (i.e. steady state):

$$Z_i(t) \to c_i B/\xi_i, \quad i = 1, 2, \dots, N.$$
 (A.2)

Hence, we may approximate each fast variable  $Z_i$  at its steady state in the slow-scale environmental bacterial equation (2.3). As a result, we obtain

$$\frac{dB}{dt} = \left[ \sum_{i=1}^{N} p_i c_i + \alpha - \delta \right] B - \frac{\alpha}{\kappa} B^2. \tag{A.3}$$

Equation (A.3) is a Bernoulli equation and can be analytically solved to obtain

$$B(t) = \left[ -\frac{d_2}{d_1} + \left( \frac{1}{B(0)} + \frac{d_2}{d_1} \right) e^{-d_1 t} \right]^{-1} \quad \text{if } d_1 \neq 0, \tag{A.4}$$

and

$$B(t) = \left[ \frac{1}{B(0)} - d_2 t \right]^{-1}, \quad \text{if } d_1 = 0, \tag{A.5}$$

where

$$d_1 = \alpha - \delta + \sum_{i=1}^{N} p_i c_i, \quad d_2 = -\frac{\alpha}{\kappa}.$$
 (A.6)

From Eqs. (A.4) and (A.5), it is clear to observe that

- (i) if  $d_1 \leq 0$ , then  $B(t) \to 0$  as  $t \to \infty$ ;
- (ii) if  $d_1 > 0$ , then  $B(t) \to -d_1/d_2$  as  $t \to \infty$ .

For case (i), Eq. (A.2) shows that  $Z_i(t) \to 0$  as  $t \to \infty$  for  $1 \le i \le N$ . This recovers the boundary equilibrium case (in the asymptotic sense) discussed in Eqs. (2.11) and (2.12). For case (ii), it leads to the positive endemic equilibrium represented in Eq. (2.10). Note that the condition  $d_1 > 0$  is equivalent to  $R_1 > 1$ , and that  $\kappa \left(1 - \frac{1}{R_1}\right) = -\frac{d_1}{d_2}$ .

## References

- [1] D. Bernstein, Matrix Mathematics (Princeton University Press, 2005).
- [2] E. Bonabeau, Agent-based modeling: Methods and techniques for simulating human systems, Proc. Natl. Acad. Sci. USA 99 (2002) 7280–7287.
- [3] L. Cai, C. Modnak and J. Wang, An age-structured model for cholera control with vaccination, Appl. Math. Comput. 299 (2017) 127–140.
- [4] L. Cai, N. Tuncer and M. Martcheva, How does within-host dynamics affect population-level dynamics? Insights from an immuno-epidemiological model of malaria, *Math. Methods Appl. Sci.* 40 (2017) 6424–6450.
- [5] V. Capasso and S. L. Paveri-Fontana, A mathematical model for the 1973 cholera epidemic in the European Mediterranean region, Rev. Epidemiol. Sante 27(2) (1979) 121–132.
- [6] R. R. Colwell, A global and historical perspective of the genus Vibrio, in *The Biology of Vibrios*, eds. F. L. Thompson, B. Austin and J. Swings (ASM Press, Washington DC, 2006).
- [7] J. Conway, Functions of One Complex Variable (Springer-Verlag, New York, 1978), pp. 322.

- [8] M. C. Eisenberg, Z. Shuai, J. H. Tien and P. van den Driessche, A cholera model in a patchy environment with water and human movement, *Math. Biosci.* 246 (2013) 105–112.
- [9] S. M. Faruque and G. B. Nair, Vibrio Cholerae: Genomics and Molecular Biology (Caister Academic Press, 2008), pp. 226.
- [10] D. M. Hartley, J. G. Morris and D. L. Smith, Hyperinfectivity: A critical element in the ability of V. cholerae to cause epidemics? PLoS Med. 3 (2006) 0063–0069.
- [11] Z. Mukandavire, S. Liao, J. Wang, H. Gaff, D. L. Smith and J. G. Morris, Estimating the reproductive numbers for the 2008–2009 cholera outbreaks in Zimbabwe, *Proc.* Natl. Acad. Sci. USA 108 (2011) 8767–8772.
- [12] R. L. M. Neilan, E. Schaefer, H. Gaff, K. R. Fister and S. Lenhart, Modeling optimal intervention strategies for cholera, Bull. Math. Biol. 72 (2010) 2004–2018.
- [13] E. J. Nelson, J. B. Harris, J. G. Morris, S. B. Calderwood and A. Camilli, Cholera transmission: The host, pathogen and bacteriophage dynamics, *Nat. Rev. Microbiol.* 7 (2009) 693–702.
- [14] M. Niazi and A. Hussain, Agent-based computing from multi-agent systems to agent-based models: A visual survey, *Scientometrics* 89 (2011) 479–499.
- [15] D. Posny and J. Wang, Modelling cholera in periodic environments, J. Biol. Dyn. 8(1) (2014) 1–19.
- [16] H. Rahmandad and J. Sterman, Heterogeneity and network structure in the dynamics of diffusion: Comparing agent-based and differential equation models, *Manag. Sci.* 54(5) (2008) 998–1014.
- [17] Z. Shuai and P. van den Driessche, Global stability of infectious disease models using Lyapunov functions, SIAM J. Appl. Math. 73 (2013) 1513–1532.
- [18] C. I. Siettos and L. Russo, Mathematical modeling of infectious disease dynamics, Virulence 4(4) (2013) 295–306.
- [19] J. H. Tien and D. J. D. Earn, Multiple transmission pathways and disease dynamics in a waterborne pathogen model, *Bull. Math. Biol.* **72**(6) (2010) 1506–1533.
- [20] X. Wang, D. Gao and J. Wang, Influence of human behavior on cholera epidemics, Math. Biosci. 267 (2015) 41–52.
- [21] J. Wang and S. Liao, A generalized cholera model and epidemic-endemic analysis, J. Biol. Dyn. 6(2) (2012) 568–589.
- [22] X. Wang and J. Wang, Analysis of cholera epidemics with bacterial growth and spatial movement, J. Biol. Dyn. 9 (2015) 233–261.
- [23] X. Wang and J. Wang, Disease dynamics in a coupled cholera model linking within-host and between-host interactions, J. Biol. Dyn. 11 (2017) 238–262.
- [24] X. Wang and J. Wang, Modeling the within-host dynamics of cholera: Bacterial-viral interaction, J. Biol. Dyn. 11 (2017) 484–501.
- [25] World Health Organization: Daily Epidemiology Bulletin, 1 October 2017.
- [26] C. Yang, X. Wang, D. Gao and J. Wang, Impact of awareness programs on cholera dynamics: Two modeling approaches, Bull. Math. Biol. 79 (2017) 2109–2131.